เอกสารอ้างอิง

[1] (http://www.westcoastrewind.com.au/images/motor7.jpg), สืบค้นวันที่ 12 สิงหาคม 2552

[2] (http://nobleengineeringservices.com.au/vibration.html), สืบค้นวันที่ 12 สิงหาคม 2552

[3] Ye, Z. and Wu, B. (2000). A Review on Induction Motor Online Fault Diagnosis.**power electronics and motion control conference, IPEMC'03**, 3, 1353 - 1358.

[4] Benbouzid, M. E. H. and Kliman, G. B. (2003). What Stator Current Processing-Based Technique to Use for Induction Motor Rotor Faults Diagnosis?.**IEEE transactions on energy conversion**,18(2),238 - 244.

[5] Thomson, W. T. and Fenger, M. (2001). Current Signature Analysis to Detect Induction Motor Faults.**IEEE industry applications magazine,7(4)**, 26 - 34.

[6] Culbert, I. M. and Rhodes, W. (2007). Current Signature Analysis Technology to Reliably Detect Cage Winding Defects in Squirrel-Cage Induction Motors.**IEEE transactions on industry applications**, 43(2), 422 - 428.

[7] Sizov, G. Y. and others. (2009). Analysis and Diagnostics of Adjacent and Nonadjacent Broken-Rotor-Bar Faults in Squirrel-Cage Induction Machines.**IEEE transactions on industrial electronics**, 56(11),4627 - 4641.

[8] Fiser, R. and Ferkolj, S. (2001). Application of a Finite Element Method to Predict Damaged Induction Motor Performance. **IEEE transactions onmagnetics**, 37(5), 3635 - 3639.

[9] Weili, L. and others. (2007). Finite-Element Analysis of Field Distribution and Characteristic Performance of Squirrel-Cage Induction Motor With Broken Bars. **IEEE transactions onmagnetics**, 43(4), 1537 - 1540.

[10] Faiz, J. and Ebrahimi, B. M. (2009). Locating Rotor Broken Bars in Induction Motors Using Finite Element Method. **Journal of energy conversion and management**, 50(1), 125 - 131.

[11] Xie, Y. (2009). Characteristic Performance Analysis of Squirrel Cage Induction Motor With Broken Bars. **IEEE transactions onmagnetics,** 45(2), 759 – 766.

[12] Schoen, R. and others. (1995). Motor Bearing Damage Detection Using Stator Current Monitoring.**IEEE transactions onindustry applications**, 31(6),
1274 - 1279.

[13] Sun, L. and Xu, B. (2007). **An improvement of stator current based detection of bearing fault in induction motors**. Retrieved December **11**, 2010, from
http://ieeexplore.ieee.org/stamp/stamp.jsp?tp=&arnumber=4348093

[14] Frosini, L.and others. (2008). **Use of the stator current for condition monitoring of bearings in induction motors**. Retrieved December **20**, 2010, from
http://ieeexplore.ieee.org/stamp/stamp.jsp?tp=&arnumber=4799991

[15] Blodt, M.and others. (2008). **Models** for Bearing Damage Detection in Induction Motors Using Stator Current Monitoring.**IEEE transactions onindustrial electronics**,55(4), 1813 - 1822.

[16] Zarei, J. and Poshtan, J. (2009). An advanced Park's vectors approach for bearing fault detection. **Science direct tribology international**, 42(2), 213 – 219.

[17] Silva, J.L.H.and Cardoso, A.J.M.(2005). **Bearing failures diagnosis in three-phase induction motors by extended park's vector approach**. Retrieved January 10, 2011, from http://ieeexplore.ieee.org/stamp/stamp.jsp?tp=&arnumber=1569315

[18] Zarei, J.and Poshtan, J.(2006). **An advanced park's vectors approach for bearing fault detection.** Retrieved January 20, 2011, from http://ieeexplore.ieee.org/stamp/stamp.jsp?tp=&arnumber=4237884

[19] Onel, I.Y.and El Hachemi Benbouzid, M. (2008).Induction Motor Bearing Failure Detection and Diagnosis: Park and Concordia Transform Approaches Comparative Study. **IEEE/ASME transactions onmechatronics**,13(2), 257 - 262.

ภาคผนวก

ภาคผนวก ก การเก็บข้อมูล

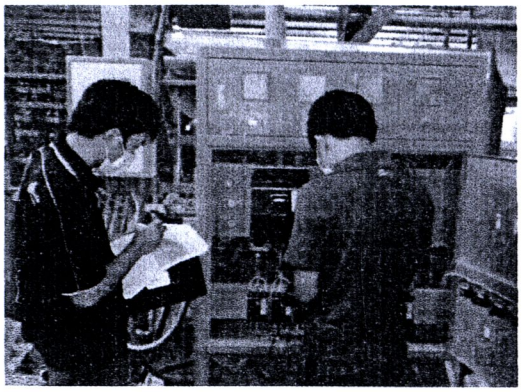

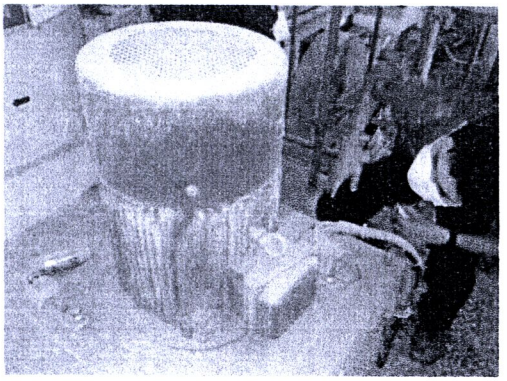

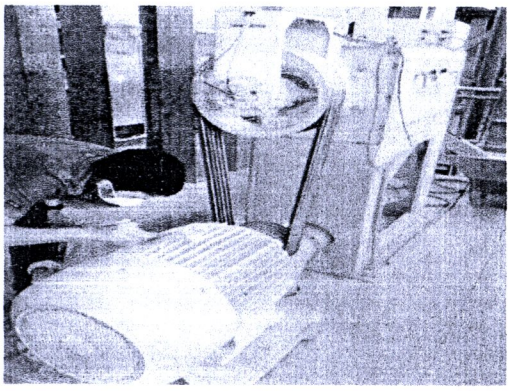

ขณะทำการเก็บข้อมูลการทำงานของมอเตอร์ไฟฟ้า ในกระบวนการสีข้าว

ภาคผนวก ข การอบรม

รายชื่อผู้ร่วมการอบรมการตรวจสอบความผิดปกติ เบื้องต้นของมอเตอร์ไฟฟ้า

ในวันที่ 19 ตุลาคม 2554 โดยมีผู้เข้าร่วมทั้งสิ้น 12 ท่าน ประกอบด้วย

1.	คุณ วีระเมธ	ชามพูนท
2.	คุณ พิษณุ	จอมประเสริฐ
3.	คุณ เครือณรงค์	ทรายคำ
4.	คุณ สุเทพ	สายยืด
5.	คุณ วุฒิพงษ์	นาหุ่น
6.	คุณ อนงค์	มหมัด
7.	คุณ บาง	นาคบุรี
8.	คุณ ประจวบ	อ่อนอุ่น
9.	คุณ ชายชาญ	อินสอน
10.	คุณ สมชาย	เรือนทิ
11	คุณ เสน่ห์	ภู่เชย
12	คุณ วิทยา	ยั่งยืน

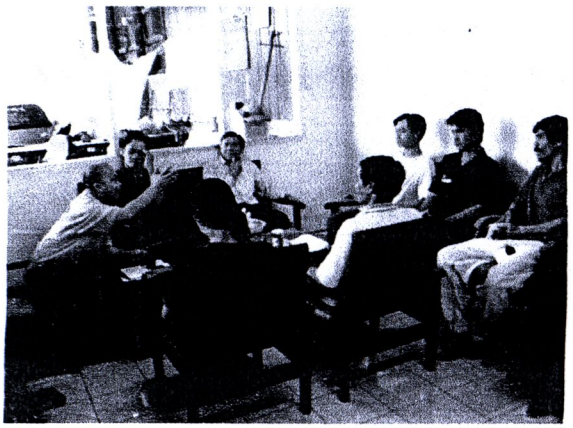

ขณะให้การแนะนำการตรวจสอบความผิดปกติ เบื้องต้นของมอเตอร์ไฟฟ้า

ภาคผนวก ข การอบรม

รายชื่อผู้ร่วมการอบรมการตรวจสอบความผิดปกติ เบื้องต้นของมอเตอร์ไฟฟ้า

ในวันที่ 20 มกราคม 2555 โดยมีผู้เข้าร่วมทั้งสิ้น 30 ท่าน ประกอบด้วย

1. นายเกรียงศักดิ์ ไกรกิจราษฎร์
2. นางสาวเดือนแรม แพ่งเกี่ยว
3. นายสิทธิพงษ์ เพ็งประเดิม
4. นายบุญญฤทธิ์ วังงอน
5. นายเกรียงศักดิ์ สุขศรี
6. นายปรเมศวร์ อนุพันธิกุล
7. นายศักดา เอี่ยมสะอาด
8. นายเศกวุฒิ ดิษฐแย้ม
9. นายบุญประเสริฐ มาบุญช่วย
10. นายกริช คงมีสุข
11. นายประวัติ นวลมีชื่อ
12. นายธนวัฒน์ ศรีตา
13. นายจักรีวุฒิ สวยงาม
14. นายอรรถวุฒิ วงศา
15. นายปรมินทร์ ตื้อคำ
16. นายอนุรักษ์ เมืองวงศ์
17. นายอนุสรณ์ ขยันกสิกรณ์
18. นายสายัญ เขียวจันทร์
19. นายภัทรวุฒิ ธรรมธีระศิษฏ์
20. นายทศพร อุปคำ
21. นายอภินันท์ บรรจร
22. นายธนากร หล้าสวย
23. นายกฤษฎา เหมบุรุษ
24. นางสาวทัศนีย พุกกะณะสูต
25. นายอัครวิศว์ อยู่พุ่มพฤกษ์
26. นายจำลอง เปล่งเพิ่มพูน

27. นายสุนทร รัตนบรรเทิง
28. นางสาววิสาวัลย์ สุขสุศรี
29. นางสาวไอลดา ทองสันทัด
30. นวยธนพัฒน์ มณฑาทิพย์

ขณะให้การแนะนำการตรวจสอบความผิดปกติ เบื้องต้นของมอเตอร์ไฟฟ้า

ภาคผนวก ค บทความสำหรับการเผยแพร่

[1] N. Sittisrijan and S. Ruangsinchaiwanich, "Synthesis of stator current waveform of induction motor", International Conference Electrical Machines and Systems (ICEMS 2011), Beijing, China, August 20-23, 2011

Analysis of Stator Current Waveforms of Induction Motor with Broken Bar Conditions

N. Sittisrijan and S. Ruangsinchaiwanich
Department of Electrical and Computer Engineering, Faculty of Engineering
Naresuan University, Muang, Phitsanuloke, 65000 Thailand.
Email: sompornru@yahoo.co.uk

Abstract — Induction motor is the main electrical machine for many applications because it has advantage sides. However, it may be affected by many problems for example the broken rotor bar problem. In recent year, many researches attempt to investigate the characteristics of induction motor with the broken rotor bar conditions. This paper aims to synthesis of stator current waveform of induction motor with broken bar conditions by using the single broken bar condition of the stator current waveform. The synthesis method can be separated as two cases, which is originated by the FEM and the experimental results. Finally, the proposed synthesize method from using the result of the experimental work can be considered successfully.

I. Introduction

Induction motors are widely used in the industrial process due to its efficiency, low maintenance, and inexpensiveness. However, long time use can cause damage to motors, particularly to the main components, e.g. bearing, stator winding, and rotor bar [1-4]. The maintenance of the induction motor is necessary for preventing the damage. If the motor is detected its fault before damage is occurred, serious loss can be prevented and motor life will be prolonged. Many researchers studied on analysis of motor fault by diagnosing stator current. The motor fault will generate harmonic stator current at different frequency depending on types of fault [3]. Some researchers used stator current analysis to diagnosing rotor bar failure in the induction motor [5-7]. Recently, researchers also used the FEM to create several motor models for studying in order to save time and cost. The FE analysis can illustrate the electromagnetic waveforms which are a normal waveform, and irregular distribution of magnetic force, [10-11,13-15]. However, some irregular electromagnetic distributions, which calculated by FEM, are required to be considered carefully [14-15].

In this paper, the squirrel cage induction motor is investigated for proposing the synthesize method to predict the stator current waveform which is caused by the broken rotor bar problem. For measurement method, the current signature analysis is selected and several broken rotor bar cases are researched for confirming the proposed synthesize method.

II. Design of 2D FEM Analysis Methodology

A. Motor parameters of FEM model

Basically, the finite element method (FEM) is a tool for diagnosing induction motor prototype, which is a single phase motor. Figure 1 shows the induction motor parameters and simple motor structure.

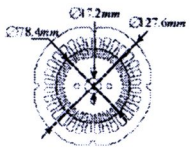

Rated power (W)	186.5
Rated voltage (V)	220
Rated frequency (Hz)	50
Number of poles	4

Fig. 1. Parameters of the motor model

B. Modeling of Broken Bars

In this paper, the squirrel-cage loops of finite element models need to be set abnormally in order to create the fracture of rotor bar circuit. Figure 3 shows the circuit setting of squirrel-cage rotor bar for both cases, which are normal and broken rotor bar conditions. Normally, the rotor bar circuit can be set simply by two different ways. Firstly, some FE program allow the FEM user to set the current to be zero in the broken bar directly, therefore the broken bar cannot effect to other circuit loops. Secondly, the material of the broken rotor bar can be replaced with non-conductive material, therefore the broken rotor bar cannot induce to any electromagnetic respond [12].

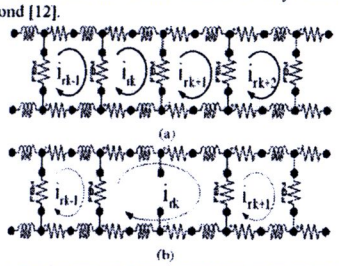

Fig. 3 The circuit setting of squirrel-cage rotor bar for the FE models (a) normal (b) a broken bar

III. Synthesis of Non-Adjacent Broken Bars Harmonic From Analysis of a Single Broken Bar

The current signature analysis is found effectively for metering diagnosing problems of the induction motor, particularly broken bar effect [1-8]. Therefore, the sideband frequencies of the induction motor with the broken bar problem can be reviewed as:

$$f_{sb} = (1 \pm 2ks) f_e \qquad (1)$$

where f_{sb} are the sideband frequencies with broken rotor bar (Hz), f_e is supply frequency (Hz), $k = 1, 2, 3, \ldots$ and s is per unit slip of motor

Fundamentally, the normal stator current waveform can be expressed as:

$$i_{mh} = \sum_{n=1,2,..}^{\alpha} I_n \sin(n\omega_s t + \theta_n) \quad (2)$$

where I_n and θ_n are the harmonic order of the peak current, and initial phase angle of the harmonic order phase current.

Moreover, in the case of the broken bar condition, the stator current waveform of a single broken bar rotor can be expressed as:

$$i_{sb} = I_{ls}\sin((1-2s)\omega_s t + \phi_{ls}) + I_{us}\sin((1+2s)\omega_s t + \phi_{us}) \quad (3)$$

where I_{ls}, I_{us} are the lower sideband component associated with the single broken bar, and the upper sideband component associated with the single broken bar, respectively, two angles ϕ_{ls} and ϕ_{us} denote the initial phase angle of the lower sideband and upper sideband components.

Typically, rotor frequency can be expressed as:

$$f_r = \frac{n_{sync} - n_m}{n_{sync}} f_e \quad (4)$$

Also, speed of the magnetic field's rotation is given by

$$n_{sync} = \frac{120 f_e}{P} \quad (5)$$

where P is the pole of the induction motor.

Therefore

$$f_r = \frac{P}{120}(n_{sync} - n_m) \quad (6)$$

From the equation (6) can be rearranged as:

$$2\pi s f_e t = p2\pi(f_{sync} - f_m)t \quad (7)$$

where f_{sync}, f_m are frequency of the magnetic field speed, and frequency of the rotor speed respectively, p is pole pairs of the induction motor.

Assuming

$$\theta = 2\pi(f_{sync} - f_m)t \quad (8)$$

Consequently

$$2\pi s f_e t = p\theta \quad (9)$$

From the equation (3), the stator current waveform of a single broken bar rotor would be directed as:

$$i_{sb} = I_{ls}\sin(\omega_s t - 2p\theta + \phi_{ls}) + I_{us}\sin(\omega_s t + 2p\theta + \phi_{us}) \quad (10)$$

Again, the stator current waveform of N_{bb} broken bar can be transformed as:

$$i_b = \sum_{k=1,2,..}^{N_{bb}} I_{ls}\sin\left(\omega_s t - 2p\left(\theta + \frac{2\pi N_k}{N_b}\right) + \phi_{ls}\right) + I_{us}\sin\left(\omega_s t + 2p\left(\theta + \frac{2\pi N_k}{N_b}\right) + \phi_{us}\right) \quad (11)$$

The equation (11) can be rearranged as:

$$i_b = \sum_{k=1,2,..}^{N_{bb}} I_{ls}\sin\left(\omega_s t - 2p\theta + \frac{2p2\pi N_k}{N_b} + \phi_{ls}\right) + I_{us}\sin\left(\omega_s t + 2p\theta + \frac{2p2\pi N_k}{N_b} + \phi_{us}\right) \quad (12)$$

Letting

$$a = \omega_s t - 2p\theta + \phi_{ls},\ b = \omega_s t + 2p\theta + \phi_{us},\ c = \frac{2\pi 2pN_k}{N_b} \quad (13)$$

Therefore

$$i_b = I_{ls}\sum_{k=1,2,..}^{N_{bb}}(\sin a\cos c + \cos a\sin c) + I_{us}\sum_{k=1,2,..}^{N_{bb}}(\sin b\cos c + \cos b\sin c) \quad (14)$$

Then

$$i_b = I_{ls}\left(\sin a\sum_{k=1,2,..}^{N_{bb}}\cos c + \cos a\sum_{k=1,2,..}^{N_{bb}}\sin c\right) + I_{us}\left(\sin b\sum_{k=1,2,..}^{N_{bb}}\cos c + \cos b\sum_{k=1,2,..}^{N_{bb}}\sin c\right) \quad (15)$$

Therefore

$$i_b = \sqrt{\left(\sum_{k=1,2,..}^{N_{bb}}\sin(c)\right)^2 + \left(\sum_{k=1,2,..}^{N_{bb}}\cos(c)\right)^2} \times\left[I_{ls}\sin\left(a + \tan^{-1}\left(\sum_{k=1,2,..}^{N_{bb}}\sin(c)\Big/\sum_{k=1,2,..}^{N_{bb}}\cos(c)\right)\right) + I_{us}\sin\left(b + \tan^{-1}\left(\sum_{k=1,2,..}^{N_{bb}}\sin(c)\Big/\sum_{k=1,2,..}^{N_{bb}}\cos(c)\right)\right)\right] \quad (16)$$

Inserting the parameters a, b and c, the resultant stator current waveforms of N_{bb} broken bar can be expressed as:

$$i_b = \sqrt{\left(\sum_{k=1,2,..}^{N_{bb}}\sin\left(\frac{2\pi 2pN_k}{N_b}\right)\right)^2 + \left(\sum_{k=1,2,..}^{N_{bb}}\cos\left(\frac{2\pi 2pN_k}{N_b}\right)\right)^2} \times\left(I_{ls}\sin(\omega_s t - 2p\theta + \phi_{ls} + \alpha) + I_{us}\sin(\omega_s t + 2p\theta + \phi_{us} + \alpha)\right) \quad (17)$$

Then

$$\alpha = \tan^{-1}\left(\sum_{k=1,2,..}^{N_{bb}}\sin\left(\frac{2\pi 2pN_k}{N_b}\right)\Big/\sum_{k=1,2,..}^{N_{bb}}\cos\left(\frac{2\pi 2pN_k}{N_b}\right)\right) \quad (18)$$

Finally, in the case of N_{bb} broken bar condition, the stator current waveforms of induction motor can be expressed as:

$$i_{mb} = \sum_{n=1,2,..}^{\alpha} I_n\sin(n\omega_s t + \theta_n) + \sqrt{\left(\sum_{k=1,2,..}^{N_{bb}}\sin\left(\frac{2\pi 2pN_k}{N_b}\right)\right)^2 + \left(\sum_{k=1,2,..}^{N_{bb}}\cos\left(\frac{2\pi 2pN_k}{N_b}\right)\right)^2} \times\left(I_{ls}\sin(\omega_s t - 2p\theta + \phi_{ls} + \alpha) + I_{us}\sin(\omega_s t + 2p\theta + \phi_{us} + \alpha)\right) \quad (19)$$

IV. EXPERIMENTAL CASE STUDIES

In this section, the case studies of the broken rotor bar motor are investigated. Figure 4 shows the photograph of the broken bar rotors which are several cases for example a healthy bar rotor, a single broken bar rotor, a two broken bars rotor, a three broken bars rotor, a four broken bars rotor and a eleven broken bars rotor respectively. Figure 5 shows laboratory measurement scene at Naresuan university.

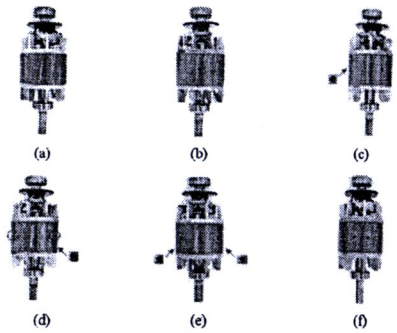

Fig. 4. Photograph of the non-adjacent broken bar rotors (a) healthy bar (b) single broken bar (c) two broken bars (d) three broken bars (e) four broken bars (f) eleven broken bars

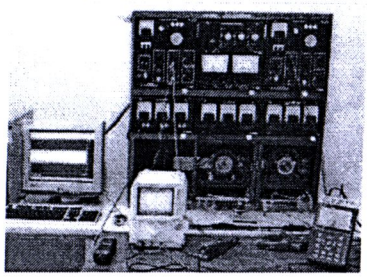

Fig. 5. Laboratory measurement scene

Firstly, the induction motor model, which has a single broken bar, is investigated by the stator current signature spectrum analysis for illustrating the fundamental sideband frequencies of motor.

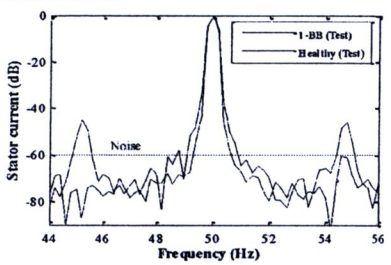

Fig. 6. Stator line current spectrum comparison

Figure 6 shows the comparison results of stator line current spectrum under the rated load condition. Since the motor has broken rotor bar, the characteristic of frequencies are normally established as $(1-2s)f_e$, which can be labeled as lower-sideband (LSB) and $(1+2s)f_e$, which can be called as upper-sideband (USB) [9-10].

A. Result of Synthesis from FEM

Figure 7 shows the amplitudes of stator current of a single broken bar at $(1-2s)f_e$ and $(1+2s)f_e$ sidebands where which is calculated by FE. Therefore their amplitudes will be employed to synthesis the stator current waveforms in other cases later. Also the study cases are separated by two groups which are the even broken bar rotor and the odd broken bar rotor.

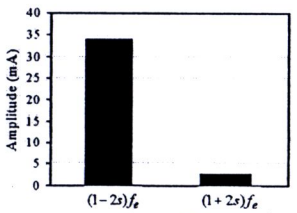

Fig. 7. Amplitude of stator current of a single broken bar calculated by FE

A1. The Even Broken Bar Rotor Case

Figure 8 shows the rotors which are a single broken bar, two broken bars and four broken bars respectively.

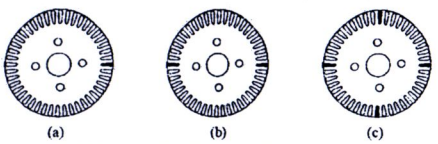

Fig. 8. The even broken bar rotor models (a) single broken bar (b) two broken bars (c) four broken bars

Figure 9 and 10 show the comparison results of the stator current waveforms by the two broken bar rotor and the four broken bar rotor motors. There are three comparable results of the stator current waveforms that are the experimental results, the proposed synthesis results and the FE calculated results. It can be seen in both figures that the stator current waveforms by the proposed synthesis and the FE calculation are similar since the proposed synthesis result is generated by the amplitudes of stator current of a single broken bar according to the equation (19) that is originally FE calculation. However, as lower-sideband (LSB), $(1-2s)f_e$, the results from all methodologies are comparable, however as upper-sideband (USB), $(1+2s)f_e$, the result from the experimental result is different. Their amplitudes of the both results from the proposed synthesis and the FE calculation are slightly lower. Figure 11 shows the comparison of their stator current amplitudes. In the even broken bar rotor case, the number of broken bar rotor is significant to the stator current amplitude [13-14].

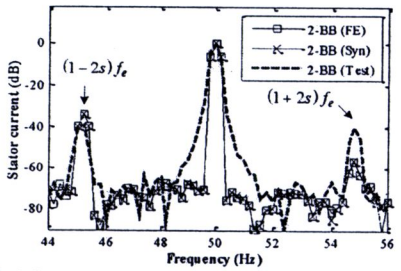

Fig. 9. Stator current spectrum comparison of the two-broken bar motor

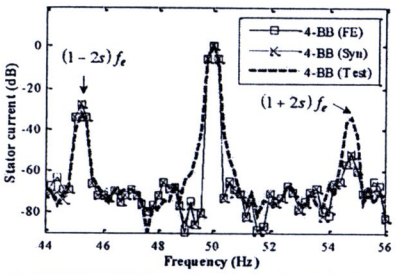

Fig. 10. Stator current spectrum comparison of the four-broken bar motor

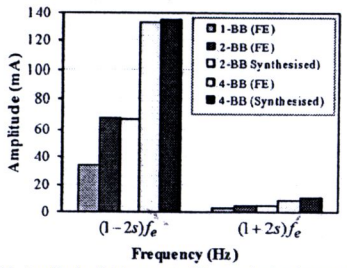

Fig. 11. Amplitude of stator current of the even broken bar motors

A2. The Odd Broken Bar Rotor Case

Figure 12 shows the rotors which are a single broken bar, three broken bars and eleven broken bars respectively.

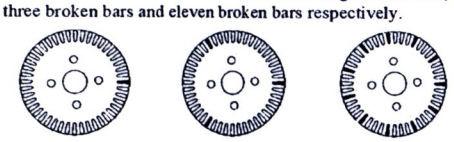

Fig. 12. The odd broken bar rotor models (a) single broken bar (b) three broken bars (c) eleven broken bars

Figure 13 and 14 show the comparison results of the stator current waveforms by the three broken bar rotor and the eleven broken bar rotor motors. Again as upper-sideband (USB), $(1+2s)f_e$, the experimental result of the stator current waveform is higher than the synthesis and FE results of stator current waveforms particularly in figure 13. However in the eleven broken bars motor their results are difficult to conclude. Since the amplitude of the current component at lower-sideband (LSB), $(1-2s)f_e$, produces generally a consequent torque pulsation at twice the slip frequency, $2sf_e$, this torque pulsation may be caused to the speed pulsations at the same frequency, therefore the amplitude of the current component at upper-sideband (USB), $(1+2s)f_e$, is very small [4]. Figure 15 shows the comparison of their stator current amplitudes. In the even broken bar rotor case, the number of broken bar rotor is also related to the stator current amplitudes, however the higher number of broken bar rotor of the induction motor can affect its lower stator current amplitude [13-14].

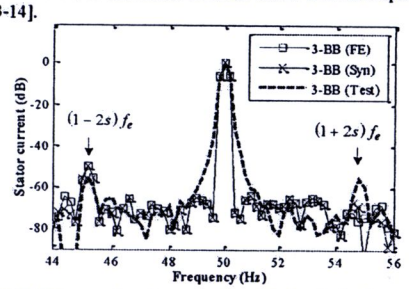

Fig. 13. Stator current spectrum comparison of the three-broken bar motor

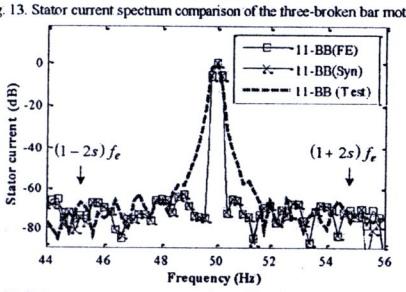

Fig. 14. Stator current spectrum comparison of the eleven-broken bar motor

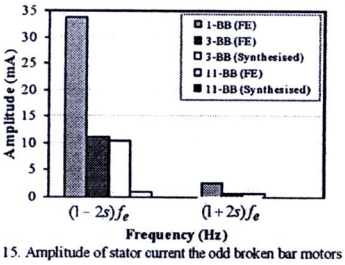

Fig. 15. Amplitude of stator current the odd broken bar motors

B. Result of Synthesis from Experimental

According a single broken bar rotor motor, the results of the amplitude current component at upper-sideband (USB), $(1+2s)f_e$, from the FE method, is small, subsequently the

proposed synthesis result of the stator current waveform is smaller than that result from the experimental work in particular at upper-sideband. In this section, the error which is caused by the FE calculation is evaded, and then the stator current waveform of a single broken bar will be focused in the experimental result. Figure 16 shows the amplitudes of stator current of a single broken bar at $(1-2s)f_e$ and $(1+2s)f_e$ sidebands where which is measured in the induction prototype. It can be notice that the amplitudes of stator current at the both sidebands are nearly equal. Therefore the proposed synthesis method according to the equation (19) will be illustrated again.

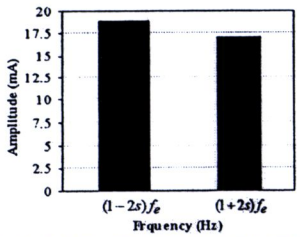

Fig. 16. Amplitude of stator current of a single broken bar from experimental

Figure 17 – 20 show the comparison results from the experimental and the proposed synthesis methods in four cases for example the two-broken bar motor, the three-broken bar motor, the four-broken bar motor and the eleven-broken bar motor respectively. Since the amplitude of the current component at upper-sideband (USB), $(1-2)s\ f_e$ (17.8 mA), is similar to the current component at lower-sideband (USB), $(1-2s)f_e$ (17.4 mA), their results are comparable.

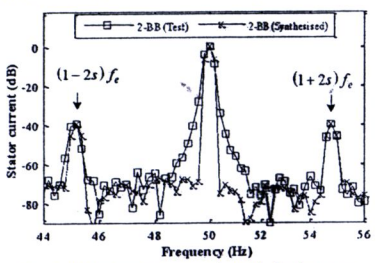

Fig. 17. Stator current spectrum the two-broken bar motor

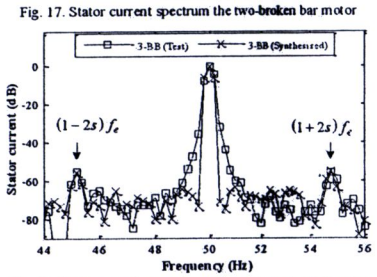

Fig. 18. Stator current spectrum of the three-broken bar motor

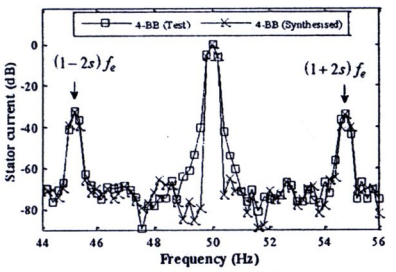

Fig. 19. Stator current spectrum of the four-broken bar motor

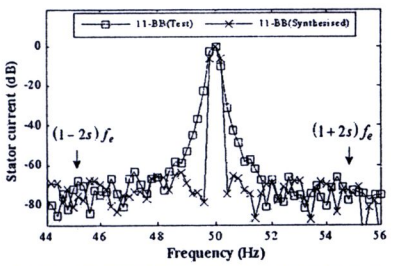

Fig. 20. Stator current spectrum of the eleven-broken bar motor

V. Conclusion

Although the predictive motor diagnosis is efficiently simulated by FEM, the error may be occurred by several reasons for example the unbalancing conditions of electromagnetic fields [15]. The broken rotor bar problem of the squirrel cage induction motor can be diagnosed by many methodologies. For example, its measurement method can be achieved effectively by the current signature analysis. The stator current waveforms of the broken rotor bar condition can be also predicted by the proposed synthesis method according by the equation (19). In particular the proposed synthesis method from the experimental work is illustrated in this paper.

VI. Acknowledgment

The authors would like to thank faulty of engineering, Naresuan University for supporting the finance for research, materials and equipments, advising staffs in this project

VII. References

[1] K. Bacha, M. Gossa, and G. A. Capolino, "Diagnosis of induction motor rotor broken bars", *IEEE International Conference on Industrial Technology 2004*, Vol.2, 8-10 Dec. 2004, Page(s): 979-982.

[2] A. Yazidi, H. Henao, and G. A. Capolino, "Broken rotor bars fault detection in squirrel cage induction machines", *IEEE International Conference on Electric Machines and Drives 2005*, 15 May 2005, Page(s): 741-747.

[3] W. T. Thomson, and M. Fenger, "Current signature analysis to detect induction motor faults", *IEEE Industry Applications Magazine*, Volume 7, Issue 4, 2001, Page(s): 26 - 34.

[4] W. Li, Y. Xie, J. Shen, and Y. Luo, "Finite-Element Analysis of Field Distribution and Characteristic Performance of Squirrel-Cage Induction

Motor With Broken Bars", *IEEE Transactions on Magnetics*, Vol. 43, No. 4, Apr. 2007, Page(s): 1537-1540.

[5] G. Y. Sizov, A. Sayed-Ahmed, Chia-Chou Yeh, and N.A.O. Demerdash, "Analysis and Diagnostics of Adjacent and Nonadjacent Broken-Rotor-Bar Faults in Squirrel-Cage Induction Machines." *IEEE Transactions on Industrial Electronics*, Volume 56, Issue 11, 2009, Page(s): 4627-4641.

[6] A. Menacer, S. Moreau, G. Champenois, M.S. N. Said, and A. Benakcha, "Experimental Detection of Rotor Failures of Induction Machines by Stator Current Spectrum Analysis in Function of the Broken Rotor Bars Position and the Load", *The international Conference on Computer as a tool (Eurocon 07)*, 9-12 Sept.. 2007, Warsaw, Poland, Page(s): 1752 – 1758.

[7] I. Culbert, and W. Rhodes, "Using current signature analysis technology to reliably detect cage winding defects in squirrel cage induction motors", Petroleum and Chemical Industry Conference 2005, Industry Applications Society 52nd Annual, 12 - 14 Sept. 2005, Page(s): 95 – 101.

[8] W. T. Thomson and M. Fenger, "Case histories of current signature analysis to detect faults in induction motor drives", in *Electric Machines and Drives Conference 2003*, Vol.3, 1-4 June 2003, Page(s): 1459-1465

[9] I. M. Culbert and W. Rhodes, "Notice of violation of IEEE publication principles using current signature analysis technology to reliably detect cage winding defects in squirrel-cage induction motors", *IEEE Transactions on Industry Applications*, Vol. 43, No.2, March/April. 2007, Page(s): 422-428 2007.

[10] J. Faiz, and B.M. Ebrahimi "Locating rotor broken bars in induction motors using finite element method", *Journal of Energy Conversion and Management*, Elsevier, Volume 50, Issue 1, 2009, Page(s): 125-131.

[11] R. Fiser, and S. Ferkolj, "Application of a finite element method to predict damaged induction motor performance." *IEEE Transactions on Magnetics*, Vol. 37, No. 5, Part 1, 2001, Page(s): 3635-3639.

[12] Y. Xie, "Characteristic Performance Analysis of Squirrel Cage Induction Motor with Broken Bars." *IEEE Transactions on Magnetics*, Vol. 45, No. 2 Part 1, 2009, Page(s): 759-766.

[13] Z. Q. Zhu, S. Ruangsinchaiwanich, and D. Howe, "Synthesis of cogging-torque waveform from analysis of a single stator slot", *IEEE Transactions on Industry Application*, Volume 42, Issue 3, May - June 2006, Page(s): 650 - 657.

[14] Z. Q. Zhu, S. Ruangsinchaiwanich, Y. Chen, and D. Howe, "Evaluation of superposition technique for calculating cogging torque in permanent-magnet brushless machines", *IEEE Transactions on Magnetics*, Volume 42, Issue 5, May 2006, Page(s): 1597 – 1603.

[15] Z. Q. Zhu, S. Ruangsinchaiwanich, and D. Howe, "Synthesis of cogging torque in permanent magnet machines by superposition", *International Power Electronics, Machines and Drives Conference (PEMD 2004)*, Edinburgh, UK, Vol. 2, 31 March - 2 April 2004, Page(s): 828 – 833

[2] N. Sittisrijan and S. Ruangsinchaiwanich, "Investigation of broken bar effect on squirrel cage induction motor by FEM", International Conference Electrical Machines and Systems (ICEMS 2010), Incheon, Korea, October 10 - 13, 2010

Investigation of the Broken Bar Effect on the Squirrel Cage Induction Motor by FEM

N. Sittisrijan and S. Ruangsinchaiwanich
Department of Electrical and Computer Engineering, Faculty of Engineering
Naresuan University, Muang, Phitsanuloke, 65000 Thailand, Email: sompornru@yahoo.co.uk

Abstract — Induction motor is the main electrical machine for many applications because it has advantage sides. However, it may be affected by many problems. This paper aims to study the broken rotor bar problem by using extensive methodologies, such as current signature analysis, magnetic vector potential, magnetic flux density and joule loss density, to investigate the broken rotor bar. Finally, the motor performances, relating to the broken rotor bar effect, are illustrated.

Index Terms—Motor Diagnosis,Induction Motor, Broken Rotor Bar

I. INTRODUCTION

Induction motors are the main component in the manufacturing process and are also widely used in household, factories, and industries. They are the important part for converting electric energy to mechanical energy in the industrial manufacturing process. Therefore, the damage of the induction motor directly affects the process, which might results in financial loss of the manufacturers.

The maintenance of the induction motor is necessary for preventing the damage. If the motor is detected its fault before damage is occurred, serious loss can be prevented and motor life will be prolonged. Many researchers studied on analysis of motor fault by diagnosing stator current. The motor fault will generate harmonic stator current at different frequency depending on types of fault [1-2]. Some researchers used stator current analysis to diagnosing rotor bar failure in the induction motor [3-5]. Recently, researchers also used the finite element method to create models or parameters for studying in order to save time and cost. The finite element analysis can illustrate collapsed electromagnetic waveform, abnormal current waveform, and irregular distribution of magnetic force, which will clearly indicate faults of motor performance [6-9].

In this paper, the squirrel cage induction motor is investigated by the predictive and measurement methods. For the predictive method, the finite element method is selected to forecast the broken bar effect on the induction motor. For measurement method, the current signature analysis and the instantaneous power spectrum analysis are picked. Also the motor performance is discussed, because the broken bar problem demolishes the motor performance in many ways.

II. DESIGN OF 2D FEM ANALYSIS METHODOLOGY

A. Fundamental Equation

The 2-D FEM model of the motor is employed and the fundamental equation describing the transient magnetic field distribution in terms of the vector magnetic potential, the reluctivity, conductivity, and current density can be expressed as [10]:

$$\frac{\partial}{\partial x}\left(\nu\frac{\partial A}{\partial x}\right)+\frac{\partial}{\partial y}\left(\nu\frac{\partial A}{\partial y}\right)=-J+\sigma\frac{\partial A}{\partial t} \qquad (1)$$

where A is the vector magnetic potential, ν is reluctivity, σ is conductivity, J is current density

B. Motor parameters of FEM model

Basically, the finite element method (FEM) is a tool for diagnosing induction motor prototype, which is a single phase motor. Figure 1 shows the induction motor parameters and simple motor structure.

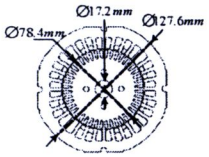

Rated power (W)	186.5
Rated voltage (V)	220
Rated frequency (Hz)	50
Number of poles	4

Fig. 1. Parameters of the motor model.

C. Modeling of Broken Bars

In this paper, the squirrel-cage loops of finite element models need to be set abnormally in order to create the fracture of rotor bar circuit. Figure 2 shows the circuit setting of squirrel-cage rotor bar for both cases, which are normal and broken rotor bar conditions. Normally, the rotor bar circuit can be set simply by two different ways. Firstly, some FE program allow the FEM user to set the current to be zero in the broken bar directly, therefore the broken bar cannot effect to other circuit loops. Secondly, the material of the broken rotor bar can be replaced with non-conductive material, therefore the broken rotor bar cannot induce to any electromagnetic respond [9].

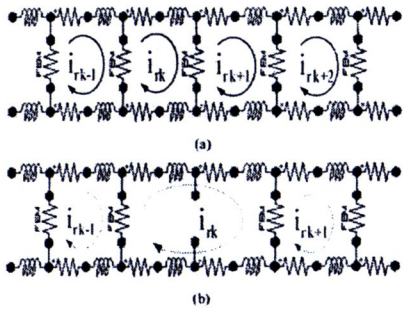

Fig. 2. The circuit setting of squirrel-cage rotor bar for the FE models (a) normal (b) a broken bar

III. Diagnostics Analysis Techniques

A. Current Signature Analysis (CSA)

The current signature analysis is found effectively for metering diagnosing problems of the induction motor, particularly broken bar effect [2-5]. Therefore, the sideband frequencies of the induction motor with the broken bar problem can be reviewed as:

$$f_{sb} = (1 \pm 2ks) f_e \tag{2}$$

where f_{sb} are the sideband frequencies with broken rotor bar (Hz), f_e is supply frequency (Hz). $k = 1, 2, 3, \ldots$ and s is per unit slip of motor.

B. Instantaneous Power Spectrum Analysis

Fundamentally, the supply voltage can be expressed as:

$$v = \sqrt{2} V \cos(\omega t + \theta_v) \tag{3}$$

where V the rms voltage and θ_v is initial phase angle of fundamental phase voltage.

Also the normal stator current waveforms can be expressed as:

$$i_h = \sqrt{2} I \cos(\omega t + \theta_i) \tag{4}$$

where I and θ_i are the rms current, and initial phase angle of fundamental phase current.

In the case of broken bar condition, the stator current waveforms can be expressed as:

$$i_b = \sqrt{2} I \cos(\omega t + \theta_i) + \sqrt{2} I_l \cos((1-2s)\omega t + \beta_l) + \sqrt{2} I_r \cos((1+2s)\omega t + \beta_r) \tag{5}$$

where I_l, I_r are the lower sideband component, and the upper sideband component, respectively, two angles β_l and β_r denote the initial phase angle of the lower sideband and upper sideband components.

Furthermore, the instantaneous power of the induction motor with the broken bar condition can be computed as:

$$\begin{aligned} p_b &= 2VI\left[\cos(\omega t + \theta_v) * \cos(\omega t + \theta_i)\right] \\ &+ 2VI_l\left[\cos(\omega t + \theta_v) * \cos((1-2s)\omega t + \beta_l)\right] \\ &+ 2VI_r\left[\cos(\omega t + \theta_v) * \cos((1+2s)\omega t + \beta_r)\right] \end{aligned} \tag{6}$$

Mathematically, the trigonometric identity is selected to apply.

$$\cos A \cos B = \frac{1}{2}\cos(A-B) + \frac{1}{2}\cos(A+B) \tag{7}$$

Eventually, the instantaneous power can be concluded as:

$$\begin{aligned} p_b &= VI\left[\cos(\theta_v + \theta_i) + \cos(2\omega t + \theta_v + \theta_i)\right] \\ &+ VI_l\left[\cos(2s\omega t + \theta_v - \beta_l) + \cos((1-s)2\omega t + \theta_v + \beta_l)\right] \\ &+ VI_r\left[\cos(2s\omega t - \theta_v + \beta_r) + \cos((1+s)2\omega t + \theta_v + \beta_r)\right] \end{aligned} \tag{8}$$

Form equation (8), frequencies of the instantaneous power harmonic due to broken bar case are induced at:

$$f_b = 2sf_e \quad \text{Hz} \qquad f_b = (1 \pm s)2f_e \quad \text{Hz} \tag{9}$$

where f_b are frequencies due to broken bars (Hz), f_e is supply frequency (Hz), s is per unit slip of motor.

IV. Experimental Case Studies

In this section, the case studies of the broken rotor bar motor are investigated. Figure 3 shows the photograph of the broken bar rotors. Also figure 4 shows laboratory measurement scene.

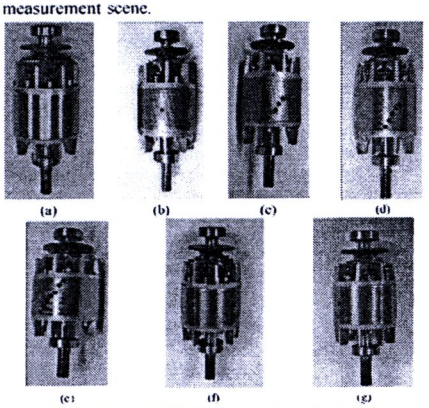

Fig. 3. Photograph of the broken bar rotors (a) healthy bar (b) single broken bars (c) three adjacent broken bar (d) five adjacent broken bar (e) seven adjacent broken bar (f) two broken bar with 180 degree separation (e) four broken bar with 90 degree separation

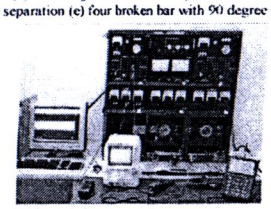

Fig. 4. Laboratory measurement scene

Firstly, the induction motor model, which has a single broken bar, is investigated by the stator current signature and instantaneous power spectrum analysis for illustrating the fundamental sideband frequencies of motor.

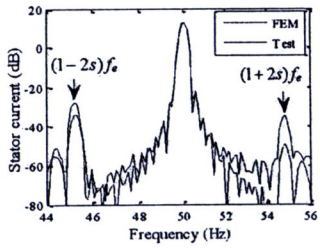

Fig. 5. Stator line current spectrum comparison

Figure 5 shows the comparison results of stator line current spectrum under the rated load condition. Since the motor has broken rotor bar, the characteristic of frequencies are normally established as $(1-2s)f_e$, which can be labeled as lower-sideband (LSB) and $(1+2s)f_e$, which can be called as upper-sideband (USB). Also, figure 6 shows the instantaneous power spectrum result. Evidently, the instantaneous power harmonics cause show both sideband of frequencies of $(1\pm s)2f_e$ and $2sf_e$, which are recognized as the frequencies of broken bars condition. Therefore, these methodologies are effective tools for investigating the broken rotor bar condition of the induction motor.

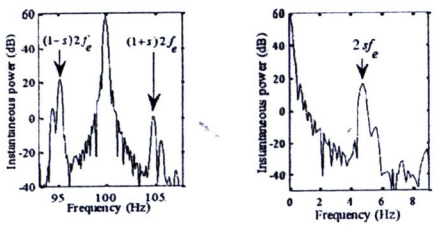

Fig. 6. Instantaneous power spectrum of faulty motor

A. Effect of the Broken Bars Position

In this section, influence of the broken bars position is investigated. Figure 7 shows the non-adjacent broken bar rotor models of FEM that are single broken bar model, two broken bar model with 180 degree separation and four broken bar model with 90 degree separation, respectively.

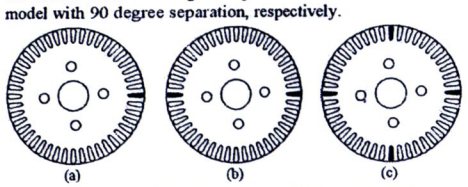

Fig. 7. Three non-adjacent broken bar models (a) single broken bar (b) two broken bars (c) four broken bars

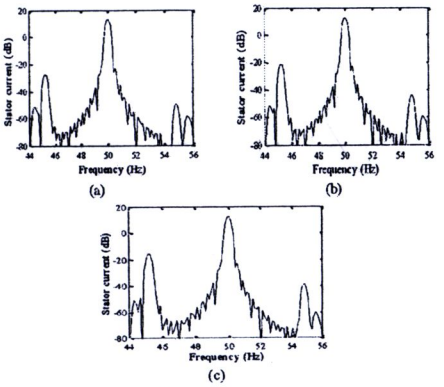

Fig. 8 Line current spectra (a) one broken bar (b) two broken bar with 180 degree separation (c) four broken bar with 90 degree separation

Figure 8 illustrates the waveforms of the stator current spectrum of the three cases. Although the sideband frequencies of these cases are found as both the $(1-2s)f_e$ and $(1+2s)f_e$, the stator current signature method in particular dB waveform unit is questioned by the influence of number of broken rotor bars. Since the increase of number of broken adjacent bars, the amplitude of harmonics of stator lines current is also increased [3][5]. Furthermore, the amplitude of harmonic components of stator current is considered as shown in table I. When number of broken nonadjacent bars is increased, according to figure 7, the amplitude of harmonic components of stator current is likely increased in both the lower and upper sidebands. For example, for the two broken bar rotor with 180 degree separation, the amplitudes of harmonic components of stator current are twice when comparing with the amplitudes of harmonic components of stator current of single broken bar rotor in both sidebands.

TABLE I
AMPLITUDES OF HARMONIC COMPONENTS OF STATOR CURRENT

Position of broken bars	$(1-2s)f_e$	$(1+2s)f_e$
Single broken bar (mA)	33.8	2.61
Two broken bar 180 degree separation (mA)	68.14	4.99
Four broken bars 90 degree separation (mA)	133.1	8.95

Morcover, the instantaneous power spectrum technique is used to study. Table II shows the amplitude results of harmonic components of power. Although the frequencies of broken bar are $(1\pm s)2f_e$, the amplitude results of harmonic components of power are significant when the number of broken rotor bar is increased, particularly non-adjacent bar position. Figure 9 shows the instantaneous power spectrum waveforms for those cases. In fact, the stator current signature and the instantaneous power spectrum analysis are directly related by considering the equation 8, therefore the results of both techniques are similar.

TABLE II

AMPLITUDES OF HARMONIC COMPONENTS OF INSTANTANEOUS POWER

Position of broken bars	$2sf_e$	$(1-s)2f_e$	$(1+s)2f_e$
Single broken bar (W)	5.24	9.93	0.84
Two broken bar 180 degree (W)	10.47	19.52	1.63
Four broken bars 90 degree (W)	20.59	37.4	2.99

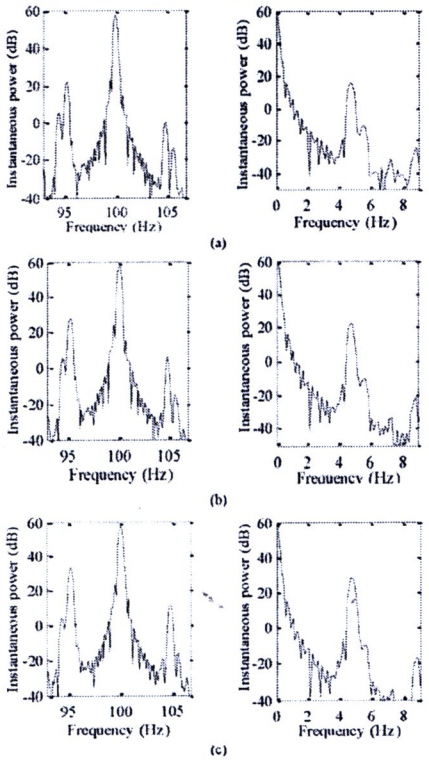

Fig. 9. Instantaneous power spectrum (a) one broken bar
(b) two broken bar with 180 degree separation
(c) four broken bar with 90 degree separation

B. *Effect of Electromagnetic Field Distribution*

In this study, the effect of electromagnetic field of the induction motor and the adjacent broken rotor bar are focused. FEM is the main tool for calculating and displaying the magnetic field distributions under the different rotor bar conditions. Figure 10 shows the comparison of magnetic field distributions of three FEM models that the motor has a healthy rotor, three adjacent broken bar and five adjacent broken bar, respectively. Under the rated load condition, the magnetic field distribution of the healthy motor is symmetrical, but the magnetic field distribution of unhealthy motor is apparently unsymmetrical.

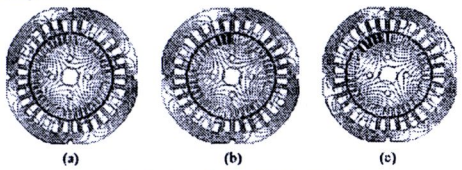

Fig. 10. Distributions of magnetic field (a) healthy rotor
(b) three adjacent broken bar (c) five adjacent broken bar

1) Magnetic Vector Potential

Figure 11 shows the results of magnetic vector potential waveforms (A) in the air-gap of the induction motors which have a healthy rotor and broken rotor bars, according to figure 10. The results of magnetic vector potential waveforms are clearly reduced because of the broken bars region. The influence of number of broken rotor bars is significant. It shows that if the motor has more number of broken rotor bars, the magnetic vector potential waveforms of motor will get more damaged. Therefore, when harmonic components of magnetic vector potential are increased, the development of inverse magnetic field, for example torque pulsation and unbalance magnetic pull will be occurred to deduce the motor performance [8].

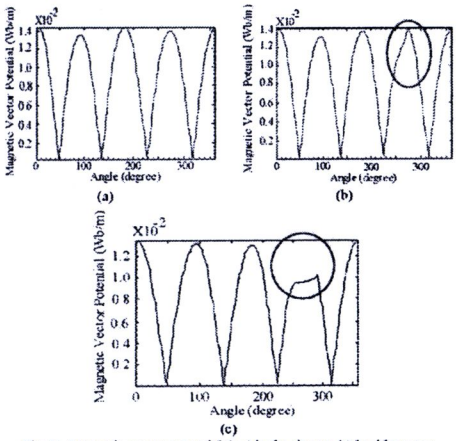

Fig. 11. Magnetic vector potential (A) in the air-gap (a) healthy rotor
(b) three adjacent broken bar (c) five adjacent broken bar

2) Magnetic Flux Density

Fundamentally, the magnetic flux density is calculated as:

$$B = \nabla \times A \tag{10}$$

Figure 12 show the results of magnetic flux density (B) in the air-gap for the induction motors which have a healthy rotor and broken rotor bars, as shown in figure 10. Since the magnetic flux density is related directly to the magnetic vector

potential, the results of the magnetic flux density calculation are damaged due to the broken rotor bar conditions.

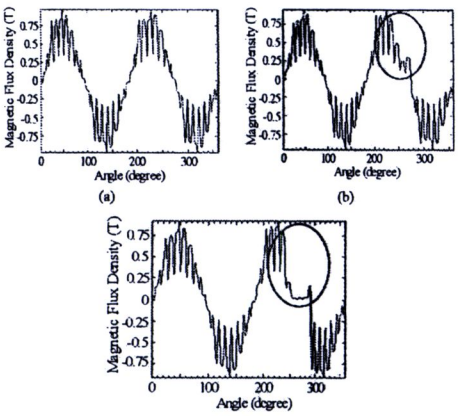

Fig. 12. Magnetic flux density (B) in the air-gap (a) healthy rotor (b) three adjacent broken bar (c) five adjacent broken bar

3) Joule Losses Density

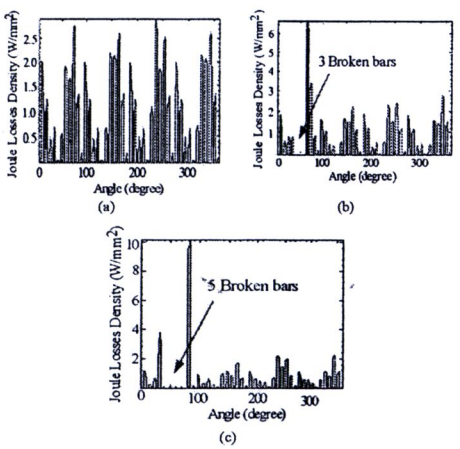

Fig. 13. Joule losses density on the rotor teeth (a) healthy rotor (b) three adjacent broken bar (c) five adjacent broken bar

In this section, Figure 13 show the results of joule losses density on the rotor teeth for the induction motor which has a healthy rotor and broken rotor bars, as shown in figure 10. There are some significant results of broken bar effect in this study. Firstly, the amplitudes of joule losses density at broken bar position are definitely diminished, and it can be clearly seen when the number of broken rotor bar is increased, for example 5 broken rotor bars as shown in Figure 13 (c). Secondly, the amplitudes of joule losses density around broken bar position are irregularly higher as shown in figure 13 (b) and (c). The amplitudes of joule losses density become 7 W/mm^2 for three adjacent broken rotor bars and 10 W/mm^2 for five adjacent broken rotor bars. Therefore, the induction motor, which has the broken rotor bar problem, particular adjacent bar case, could become more susceptible to thermal stress and eventually lead to further rotor bar degradation [7].

C. Effect of Motor Performance

Generally, the electromagnetic torque is determined by integration of T over the stator and rotor surface as:

$$T_e = \frac{rl}{\mu_0}\oint_s B_n B_t \, ds \qquad (11)$$

where B_n and B_t are the radial and tangential components of the magnetic flux density.

Since the electromagnetic torque is directly associated to the magnetic flux density, the effect of the broken rotor bar problem in the motor is continuous transferred to its electromagnetic torque. Figure 14 shows the comparison of results of electromagnetic torque waveforms between the healthy rotor bar and the five adjacent broken rotor bar effect.

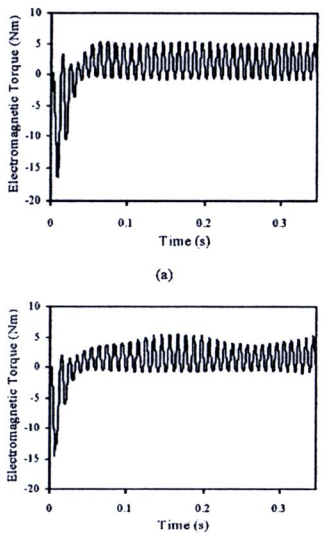

Fig. 14. Time variations of electromagnetic torque (a) healthy rotor (b) five adjacent broken bar

Correspondingly, Figure 15 and 16 show the comparison of results of motor performances with effect of rotor bar conditions. It can be stated that the broken rotor bar problem influences motor performances since their magnetic filed is demolished either its shape or amplitude. Figure 17 and 18 show the comparison of results from the FEM calculation and

the experimental results when the motors has healthy rotor bar and five adjacent broken rotor bar.

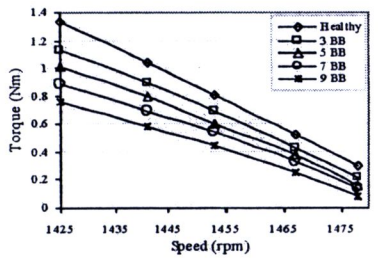

Fig. 15. Torque comparison

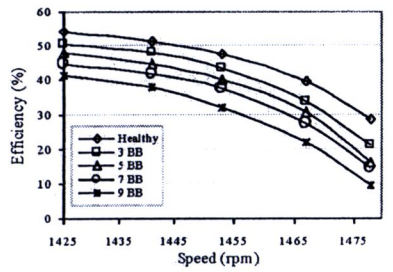

Fig. 16. Efficiency comparison

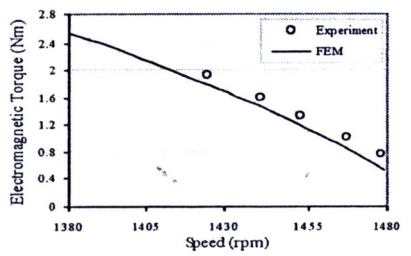

Fig. 17. Electromagnetic torque comparison with healthy rotor

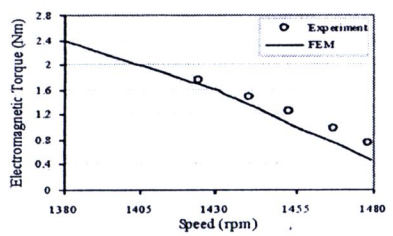

Fig. 18. Electromagnetic torque comparison with five adjacent broken bar

V. Conclusion

The broken rotor bar problem of the squirrel cage induction motor can be diagnosed by many methodologies. For example, its measurement method can be achieved effectively by the current signature analysis and the instantaneous power spectrum analysis. Moreover, the predictive motor diagnosis is efficiently simulated by FEM. Also, the broken rotor bar problem can directly effect on motor performances which are torque and efficiency. Obviously, the comparison results of the predictive FEM and the measurement method are similar. Thus, it can be concluded that the FEM calculation is the effective tool for investigating the electrical machines performance, even though the electromagnetic flied of the induction motor is damaged inconsistently.

Acknowledgement

The authors would like to thank faulty of engineering, Naresuan University for supporting the finance for research, materials and equipments, advising staffs in this project

References

[1] M. E. H. Benbouzid, and G. B. Kliman, "What stator current processing-based technique to use for induction motor rotor faults diagnosis", *IEEE Transactions on Power Engineering Review*, Volume 22, Issue 8, August 2002, Page: 62.

[2] W. T. Thomson, and M. Fenger, "Current signature analysis to detect induction motor faults", *IEEE Industry Applications Magazine*, Volume 7, Issue 4, 2001, Page(s): 26 - 34.

[3] A. Menacer, S. Moreau, G. Champenois, M.S. N. Said, and A. Benakcha, "Experimental Detection of Rotor Failures of Induction Machines by Stator Current Spectrum Analysis in Function of the Broken Rotor Bars Position and the Load", *The international Conference on Computer as a tool (Eurocon 07)*, 9-12 Sept.. 2007, Warsaw, Poland, Page(s): 1752 - 1758.

[4] I. Culbert, and W. Rhodes, "Using current signature analysis technology to reliably detect cage winding defects in squirrel cage induction motors", Petroleum and Chemical Industry Conference 2005, Industry Applications Society 52nd Annual, 12 - 14 Sept. 2005, Page(s): 95 – 101.

[5] G. Y. Sizov, A. Sayed-Ahmed, Chia-Chou Yeh, and N.A.O. Demerdash, "Analysis and Diagnostics of Adjacent and Nonadjacent Broken-Rotor-Bar Faults in Squirrel-Cage Induction Machines." *IEEE Transactions on Industrial Electronics*, Volume 56, Issue 11, 2009, Page(s): 4627-4641.

[6] J. Faiz, and B.M. Ebrahimi "Locating rotor broken bars in induction motors using finite element method", *Journal of Energy Conversion and Management*, Elsevier, Volume 50, Issue 1, 2009, Page(s): 125-131.

[7] W. Li, Y. Xie, J. Shen, and Y. Luo, "Finite-Element Analysis of Field Distribution and Characteristic Performance of Squirrel-Cage Induction Motor With Broken Bars", *IEEE Transactions on Magnetics*, Vol. 43, No. 4, Apr. 2007, Page(s): 1537-1540.

[8] R. Fiser, and S. Ferkolj, "Application of a finite element method to predict damaged induction motor performance." *IEEE Transactions on Magnetics*, Vol. 37, No. 5, Part 1, 2001, Page(s): 3635-3639.

[9] Y. Xie, "Characteristic Performance Analysis of Squirrel Cage Induction Motor with Broken Bars." *IEEE Transactions on Magnetics*, Vol. 45, No. 2 Part 1, 2009, Page(s): 759-766.

[10] A.B.J. Reece and T.W. Preston, Finite Element Methods in Electrical Power Engineering, 1st editor. Great Britain: Oxford University Press, 2000